C. Jacq
SNECMA,
direction technique,
Centre de Villaroche,
77550 Moissy Cramayel, France

D. Nélias
e-mail: daniel.nelias@insa-lyon.fr
Laboratoire de Mécanique des Contacts
(CNRS UMR 5514),
Institut national des sciences appliquées,
69621 Villeurbanne Cedex, France

G. Lormand
Groupe d'Etude Métallurgie Physique et
Physique des Matériaux (CNRS UMR 5510),
Institut national des sciences appliquées,
69621 Villeurbanne Cedex, France

D. Girodin
SNR Roulements,
BP 2017, 74010 Annecy, France

Development of a Three-Dimensional Semi-Analytical Elastic-Plastic Contact Code

A three-dimensional elastic-plastic contact code based on semi-analytical method is presented and validated. The contact is solved within a Hertz framework. The reciprocal theorem with initial strains is then introduced, to express the surface geometry as a function of contact pressure and plastic strains. The irreversible nature of plasticity leads to an incremental formulation of the elastic-plastic contact problem, and an algorithm to solve this problem is set up. Closed form expression, which give residual stresses and surface displacements from plastic strains, are obtained by integration of the reciprocal theorem. The resolution of the elastic-plastic contact using the finite element (FE) method is discussed, and the semi-analytical code presented in this paper is validated by comparing results with experimental data from the nano-indentation test. Finally, the resolution of the rolling elastic-plastic contact is presented for smooth and dented surfaces and for a vertical or rolling loading. The main advantage of this code over classical FE codes is that the calculation time makes the transient analysis of three-dimensional contact problems affordable, including when a fine mesh is required. [DOI: 10.1115/1.1467920]

Introduction

For aeronautic rolling bearings, the rolling contact fatigue (RCF) is of primary interest since it affects the durability and reliability of the aircraft engine. In those applications, bearings are designed so that loads stay below the endurance limit. This endurance limit depends upon several factors. Lamagnère et al. [1] have made a comprehensive description of the way to determine the endurance limit based on a comparison between the maximum shear stress and the microyield stress. The determination of endurance limit in RCF requires both an accurate knowledge of the stress field history and of the yield stress of the material. For those applications, an important problem is that of contact with dented surfaces. When a dent (geometrical defect of a few microns depth over a few hundred microns width) is in the contact area (few square millimetres), the contact pressure field is strongly modified from the smooth contact case, and high local pressure peaks appear around the dent. The elastic analysis of the dented contact shows that yield stress is usually exceeded, and that as it is observed experimentally plastic flow occurs. As a dent is rolled over by a rolling body, plastic strains appear, geometry and contact pressure evolve, plastic strain generates residual stress and the material is hardened. Therefore, to get a comprehensive understanding of the RCF for dented contact, it is necessary to take plasticity in the dented contact simulation into account to accurately know how stress field and the hardened yield stress changed. A tool that can simulate three dimensional elastic-plastic contact is needed.

This tool must take the evolution of contact pressure and of the stress field with plastic flow into account. Since plasticity is history dependent, the loading path must be followed analytically. Therefore, the tool has to allow for vertical loading or unloading, but also transient rolling of the bodies in contact, to simulate the rolling over the dented surface. Last, this tool must allow for a fine meshing of the contact area to take into account the presence of localized surface defects (dents) in a larger contact area. In the applications, plastic strains are considered moderate (small strains hypothesis is assumed), and plastic volumes are assumed small and surrounded by a large elastic area. Moreover the contact dimensions are small compared to the size of the bodies in such a manner that bodies may be considered as half-spaces (Hertz assumption).

The rough contact problem has been studied for many years because of its numerous implications in tribology: friction, wear, fatigue and damage. Recent review articles on contact mechanics (Barber and Ciavarella, [2]) and tribology (Tichy and Meyer, [3]) discuss many important phenomena of tribological contact and emphasize the importance of understanding the effects of roughness and plasticity. Modeling these effects has taken two main paths. The statistical approach to rough contact problems, investigated by Archard [4] and Greenwood and Williamson [5], yields important results concerning the behavior at the contact scale (contact area, normal approach). Simple plasticity ideas have recently been incorporated into this approach (Zhao et al., [6]). However, statistical models cannot predict the distribution of contact spots, local pressure or stress values, which play a major role in material fatigue and damage. Several studies have been focused on the elastic-plastic contact problem. Hahn et al. [7], and Gupta et al. [8] used a finite element approach. If a three-dimensional problem with a dented surface is considered, this kind of approach is time-consuming, as pointed out by Dang Van and Maitournan [9] because of the refinement needed for the mesh. When the plastic volume is small compared with the large elastic surrounding area, semi-analytical approaches seem to be suitable, particularly when the small strain assumption can be assumed. However, most authors use restrictive assumptions to simplify the problem. Hearle and Johnson [10] consider only plastic shear strains, Dang Van and Maitournan [9] consider a steady-state problem, so the dented contact cannot be treated because of the rolling movement of the bodies in contact. Virmoux et al. [11] have used a fast method to evaluate the elastic-plastic evolution of the contact which does not consider the pressure modification nor the rolling loading history. Finally Mayeur et al. [12] have developed a model without simplification, based on the boundary integral formulation, however restricted to two dimensional analysis.

In another way, tribologists and bearing manufacturers and users, for whom one main goal is the determination of the fatigue life of the bearing, have developed fast and robust techniques to solve the problem of dry or elastohydrodynamically lubricated contact between two real surfaces (with measured surface roughness). Current methods using the Fast Fourier Transform (Polon-

Contributed by the Tribology Division for publication in the ASME JOURNAL OF TRIBOLOGY. Manuscript received by the Tribology Division June 13, 2001; revised manuscript received November 2, 2001. Associate Editor: M. D. Bryant.

sky and Keer [13]) or the Multigrid Multi Integration techniques (Lubrecht and Ioannides [14]) are now fast enough to permit transient simulation of a surface defect rolling through the contact. However such approaches, which are based on the elastic half-space theory lead to purely elastic analysis while contact pressures leading to stresses up to several times the yield stress of the material are locally found.

In the last developments where plasticity has been included in the transient analysis of contact between non-smooth surfaces two papers may present some interest for the readers. Xu et al. [15] were able to calculate the residual stresses due to debris in EHL contacts, but the model was limited to line contact problems (two-dimensional analysis). Very recently Liu et al. [16] have presented a refined model that accounted also for thermo-elastic deformations (three-dimensional thermo-elasto-plastic model for dry contact with rough surfaces), where plasticity was considered only as a limiting maximum contact pressure. It should be noted that both teams used the FEM to solve the contact problem.

In order to overcome these difficulties, a numerical method based on a boundary integral formulation for an elastoplastic half-space is presented in this paper. The method is applied to three-dimensional elastoplastic contact problems with Von-Mises yielding and isotropic hardening. This new numerical method, which is an extension of the method presented by Mayeur et al. [12], requires discretization of only the contact surface and plastic zone. Thus, the numerical system is dramatically smaller than the bulk discretization of finite element systems. Also, the numerical system is well suited for an FFT-based scheme that was used to increase the speed of computation.

The semi-analytical code (SAC) presented here can not only solve problems with vertical loading but also those with moving loads (also called transient rolling elastic-plastic contact), with smooth or dented contacting bodies. The principal goal of this paper is to give an overview of the theory in such a manner than other researchers could rebuild an equivalent computing code. The main assumptions (or limitations) of the proposed analysis are those of small strains and rotations, and semi-infinite bodies. However, the problem is well-adapted to contact problems with high resistance steels, such as bearing steels. The present model has already been used to determine the micro-yield stress profile versus depth of a surface hardened material by the inverse method from nano-indentation experiments [17]. Further application to RCF of dented surface will be presented in a future paper.

The theory is presented in the first part. It leads to an incremental formulation of the elastic-plastic contact problem. In the second part, numerical tools are set up to enable the resolution of the problem. Finally several academic applications are presented. The first one consists of a vertical loading which is also used to validate the SAC by comparing results supplied by the commercial finite elements code ABAQUS. The vertical loading of a dented surface, the rolling on a smooth surface and finally the rolling over a dent are presented to illustrate the capabilities of the SAC, as required to get a comprehensive description of the RCF for dented surfaces.

1 Formulation of the Elastic-Plastic Contact Problem. Resolution Algorithm.

The work presented in this paper remains within the framework of Hertz's hypotheses. Small strains are assumed, and the dimensions of the contact area are small with regard to the radii of curvature of the contacting bodies that can be considered as half-spaces. The contact is subjected to normal loading and tangential effects are neglected. The problem is three-dimensional and no symmetry is implicitly taken into account. Symbols σ and ε denotes respectively the stress and the strain tensors; ε^e, ε^p, and ε^o represent the elastic, the plastic and the initial strain tensors; u is the displacement vector; and M_{ijkl} is the fourth order elastic constant tensor.

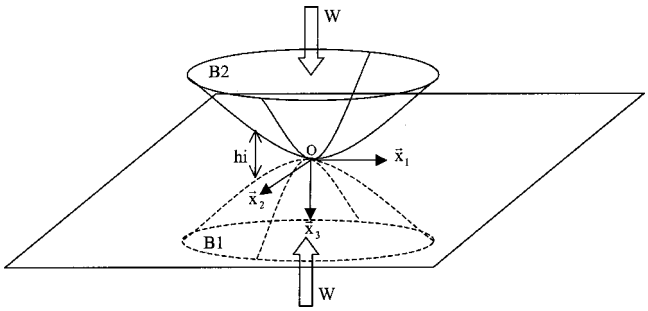

Fig. 1 Contact problem description

1.1 Contact Formulation. A dry static or quasi static normal contact problem between two bodies B1 and B2 (Figs. 1 and 2) can be described by a set of equations that must be solved simultaneously. These equations are:

- *The load balance*. The integration of contact pressure $p(x_1,x_2)$ must be equal to the applied external load W. The part of the surface where the pressure is not nil is called Γ_c.

$$W=\int_{\Gamma_c} p(x_1,x_2)d\Gamma\,. \tag{1.1}$$

- *The surface separation*. The distance between the contacting surfaces $h(x_1,x_2)$ is defined by the initial geometry $hi(x_1,x_2)$, the rigid body displacement δ and by the surface normal displacements of both bodies $u_3^{(B1+B2)}(x_1,x_2)$:

$$h(x_1,x_2)=hi(x_1,x_2)+\delta+u_3^{(B1+B2)}(x_1,x_2)\,. \tag{1.2}$$

- *The contact conditions*. The bodies cannot interpenetrate one another; thus $h(x_1,x_2)$ must be positive or nil. If $h(x_1,x_2)$ is not nil, no contact occurs and no pressure is transmitted:

$$h(x_1,x_2)\geqslant 0 \quad \text{and} \quad p(x_1,x_2)\geqslant 0$$
$$\text{if } h(x_1,x_2)>0 \text{ then } p(x_1,x_2)=0\,. \tag{1.3}$$

This set of equations can be solved if the surface normal displacement $u_3^{(B1+B2)}(x_1,x_2)$ can be expressed as a function of the contact pressure. The reciprocal theorem will be used to fulfill this condition for the elastic-plastic contact problem.

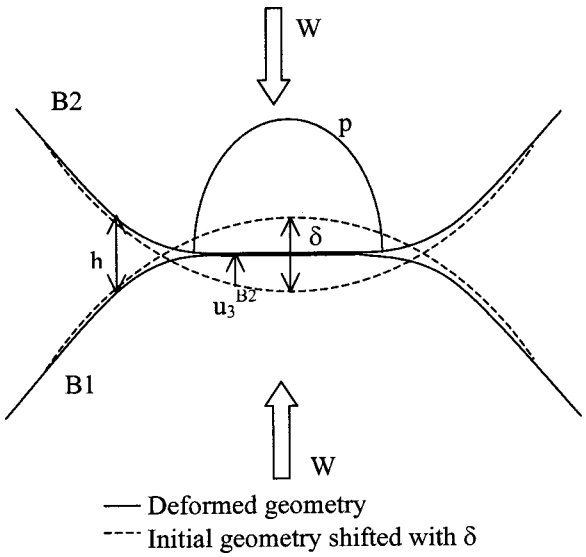

Fig. 2 Surface separation. Representation in the plane $(0,\vec{x}_1,\vec{x}_3)$.

1.2 Reciprocal Theorem. Consider two independent loads applied to an elastic body of volume Ω and of boundary Γ. The first state, noted $(u,\varepsilon,\sigma,f_i)$ exists with initial strains ε^0. The second state, noted $(u^*,\varepsilon^*,\sigma^*,f_i^*)$ is for the moment undefined (Brebbia, [18]; Mayeur, [19]).

- Consider the product

$$\sigma_{ij}.\varepsilon_{ij}^*=M_{ijkl}.(\varepsilon_{kl}-\varepsilon_{kl}^0)\varepsilon_{ij}^*. \tag{1.4}$$

- Because of the symmetry of the tensors,

$$\sigma_{ij}.\varepsilon_{ij}^*=(\varepsilon_{kl}-\varepsilon^0{}_{kl})\sigma_{kl}^*. \tag{1.5}$$

- Integrate (1.5) on the domain Ω. Left part of (1.5).

$$\int_\Omega \sigma_{ij}\varepsilon_{ij}^* d\Omega=\int_\Omega \frac{\sigma_{ij}}{2}(u_{i,j}^*+u_{j,i}^*)d\Omega. \tag{1.6}$$

- Because of the symmetry of the stress and strain tensors, one can write

$$\int_\Omega \sigma_{ij}\varepsilon_{ij}^* d\Omega=\int_\Omega \sigma_{ij}u_{i,j}^* d\Omega=\int_\Omega (\sigma_{ij}u_i^*)_{,j}d\Omega-\int_\Omega \sigma_{ij,j}u_i^* d\Omega. \tag{1.7}$$

Equilibrium conditions being satisfied,

$$\int_\Omega \sigma_{ij}\varepsilon_{ij}^* d\Omega=\int_\Omega (\sigma_{ij}u_i^*)_{,j}d\Omega+\int_\Omega f_i u_i^* d\Omega. \tag{1.8}$$

- By applying the theorem of Ostrogradski with n_j the entering normal unit vector:

$$\int_\Omega \sigma_{ij}\varepsilon_{ij}^* d\Omega=-\int_\Gamma u_i^*\sigma_{ij}n_j d\Gamma+\int_\Omega f_i u_i^* d\Omega. \tag{1.9}$$

- Right part of (1.5).

$$\int_\Omega (\varepsilon_{ij}-\varepsilon_{ij}^0)\sigma_{ij}^* d\Omega=\int_\Omega \varepsilon_{ij}\sigma_{ij}^* d\Omega-\int_\Omega \varepsilon_{ij}^0\sigma_{ij}^* d\Omega. \tag{1.10}$$

Using the theorem of Ostrogradski:

$$\int_\Omega (\varepsilon_{ij}-\varepsilon_{ij}^0)\sigma_{ij}^* d\Omega=-\int_\Gamma u_i\sigma_{ij}^* n_j d\Gamma+\int_\Omega f_i^* u_i d\Omega-\int_\Omega \varepsilon_{ij}^0\sigma_{ij}^* d\Omega. \tag{1.11}$$

- Finally, the reciprocal theorem with initial strains can be written as

$$-\int_\Gamma u_i^*\sigma_{ij}n_j d\Gamma+\int_\Omega f_i u_i^* d\Omega=-\int_\Gamma u_i\sigma_{ij}^* n_j d\Gamma+\int_\Omega f_i^* u_i d\Omega-\int_\Omega \varepsilon_{ij}^0\sigma_{ij}^* d\Omega \tag{1.12}$$

1.3 Application of the Reciprocal Theorem to Surface Displacement Calculation. The reciprocal theorem is applied to both bodies in contact, where each of them is considered as a half-space Ω whose boundary Γ is loaded on a part Γ_C. Initial strains occupy a volume Ω_p. Since $\sigma_{ij}n_j=-p_i$ Eq. 1.12 becomes:

$$\int_{\Gamma_c} u_i^* p_i d\Gamma=\int_\Gamma u_i p_i^* d\Gamma+\int_\Omega f_i^* u_i d\Omega-\int_{\Omega_p}\varepsilon_{ij}^0\sigma_{ij}^* d\Omega. \tag{1.13}$$

If the initial strains are plastic strains $(\mathrm{tr}(\varepsilon^p)=0)$, one demonstrates easily that:

$$\int_{\Gamma_c} u_i^* p_i d\Gamma=\int_\Gamma u_i p_i^* d\Gamma+\int_\Omega f_i^* u_i d\Omega-2\mu\int_{\Omega_p}\varepsilon_{ij}^p\varepsilon_{ij}^* d\Omega. \tag{1.14}$$

Consider the state $(u^*,\varepsilon^*,\sigma^*)$ corresponding to the application of a unit force along $\vec{x}_3$ applied on the elementary surface area centred at point A of the surface, while neglecting body forces $(f^*=0)$, leading to pressure $p^*(M)=(0,0,0)$ if $M\neq A$ and $p^*(M)=(0,0,1/(dx_1dx_2))$ if $M=A$. It is called $(u^*(M,p^*(A)),\varepsilon^*(M,p^*(A)),\sigma^*(M,p^*(A))$. Equation 1.14 then becomes:

$$\begin{aligned}u_3(A)&=\int_\Gamma u_i(M)p_i^*(M)d\Gamma\\&=\int_{\Gamma_c} u_i^*(M,p^*(A))p_i(M)d\Gamma\\&\quad+2\mu\int_{\Omega_p}\varepsilon_{ij}^p(M)\varepsilon_{ij}^*(M,p^*(A))d\Omega\end{aligned} \tag{1.15}$$

with M a point of the integration surface or volume.

The surface normal displacement of each body can then be expressed as a function of contact pressure and of plastic strain existing in the considered body. The authors now consider only one body in contact with an elastic-plastic behavior, the other one being purely elastic. The formulation could be extended to the case of two elastic-plastic bodies without major difficulties.

To solve this contact problem, it is necessary to relate the surface displacement to the contact pressure. In expression 1.15, the displacement is related to the contact pressure (as in the elastic case), but also to the plastic strains. It is then necessary to express the plastic strains as a function of contact pressure.

1.4 Application of the Reciprocal Theorem to Stress Calculation. Plastic strains are related to stresses. Therefore, the stress field must be evaluated from elastic-plastic contact conditions. Consider the reciprocal theorem applied to a half-space Ω whose boundary Γ is loaded on a part Γ_C as in paragraph 1.3, Eq. 1.14. Consider now the state $(u^{**},\varepsilon^{**},\sigma^{**})$, corresponding to a body force applied at a point B of the half-space in the direction k and of magnitude one.

$$\int_\Omega f_i^{**}u_i d\Omega=u_k(B);\qquad \int_\Gamma u_i p_i^{**}d\Gamma=0. \tag{1.16}$$

Equation 1.14 then becomes:

$$\begin{aligned}u_k(B)&=\int_{\Gamma_c} u_i^{**}(M,B).p_i(M)d\Gamma\\&\quad+2\mu\int_{\Omega_p}\varepsilon_{ij}^p(M).\varepsilon_{kij}^{**}(M,B)d\Omega.\end{aligned} \tag{1.17}$$

Stresses can be related to the displacements via Hooke's law. Therefore, the stress at every point of the half-space can be divided in two parts, $\sigma=\sigma^{pr}+\sigma^r$. In the first term, the pressure stress is linked to the contact pressure, while the residual stress is related to the plastic strains in the second term. The residual stress is the stress induced by the strain nuclei. It is also the stress produced by plastic strain remaining after unloading, i.e., $p_i(M)=0$ in Eq. 1.17.

This relation shows that the stress field changes with plastic flow, primarily due to the appearance of plastic strains, but also because of the modification of contact pressure due to geometry changes.

This method has some similarities with the work presented by Blomerus et al. [20], who have developed a method in which distributed dislocations are used to model plasticity in two-dimensional problems.

1.5 Plasticity Model. Plasticity is an irreversible phenomenon, that requires an incremental description. In a general incremental formulation of plasticity, a plastic strain increment depends upon the stress, the stress increment and upon the hardening parameters:

$$\delta\varepsilon^p = f(\sigma, \delta\sigma, \text{ hardening parameters}) . \tag{1.18}$$

This general formulation is used for theoretical development. The chosen plasticity model is described in the third part of this paper, concerned with the validation of the SAC.

1.6 Incremental Formulation of Elastic-Plastic Contact. Since plasticity is an irreversible phenomena, the relation between plastic strain and contact pressure must also be incremental. Therefore, an incremental formulation of the elastic-plastic contact problem must be used:

- *Initial conditions.*

$$W, hi(x_1,x_2), p(x_1,x_2), \varepsilon^p, \text{ hardening parameters} \tag{1.19}$$

- *Load balance.*

$$W + \delta W = \int_{\Gamma_c} [p(x_1,x_2) + \delta p(x_1,x_2)] d\Gamma \tag{1.20}$$

- *Surface separation.*

$$h(x_1,x_2) = hi(x_1,x_2) + \delta + u_3^{pr(B1+B2)}(x_1,x_2) + u_3^r(x_1,x_2) + \delta u_3^r(x_1,x_2) \tag{1.21}$$

$$u_3^{pr}(A) = \int_{\Gamma_c} u_{3i}^*(M,A).(p_i + \delta p_i)(M) d\Gamma: \text{ displacement due to contact pressure} \tag{1.22}$$

$$u_3^r(A) = 2\mu \int_{\Omega_p} \varepsilon_{ij}^p(M) \varepsilon_{3ij}^*(M,A) d\Omega: \text{ displacement due to plastic strain} \tag{1.23}$$

$$\delta u_3^r(A) = 2\mu \int_{\Omega_p} \delta\varepsilon_{ij}^p(M) \varepsilon_{3ij}^*(M,A) d\Omega: \text{ displacement due to } \delta\varepsilon^p \tag{1.24}$$

- *Plasticity model.*

$$\delta\varepsilon^p = f(\sigma, \delta\sigma, \text{ hardening parameters})$$

- *Stress calculation.*

$$\sigma = \sigma^{pr}(p) + \sigma^r(\varepsilon^p)$$
$$\delta\sigma = \delta\sigma^{pr}(\delta p) + \delta\sigma^r(\delta\varepsilon^p) \tag{1.25}$$

- *Contact conditions.*

$$h(x_1,x_2) \geqslant 0$$
$$\text{if } h(x_1,x_2) > 0 \text{ then } p(x_1,x_2) + \delta p(x_1,x_2) = 0 . \tag{1.26}$$

To complete this incremental formulation, the loading history must be defined. Two types of load increments are considered (Fig. 3). The first one is a vertical loading or unloading without rolling movement. The only change is an increase or a decrease of the applied external load *W*. The second type of load increment corresponds to a rolling movement of the load. The applied external load does not change. Considering a mark attached to the contact, the plastic strain, hardening state and contact pressure *p* must be shifted. The initial geometry $hi(x_1,x_2)$ can also evolve, as it is the case in Fig. 3, where a surface defect is entering the contact zone, as the bodies in contact are rolling, which indeed will strongly modify the contact pressure distribution.

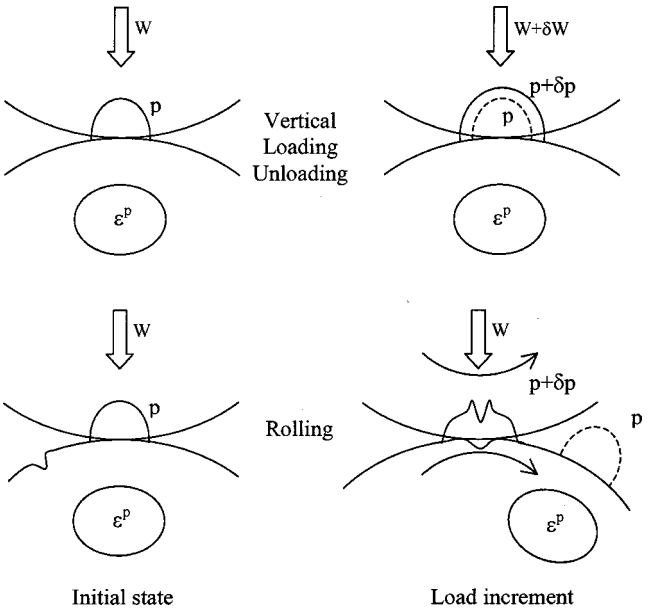

Fig. 3 Load history description

It can also be noted that if ε^p and $\delta\varepsilon^p$ are known in Eq. 1.21, this contact formulation is that of the elastic contact, with a modified initial geometry $himod = hi + u_3^r + \delta u_3^r$. This will be used for the elastic-plastic contact resolution.

1.7 Resolution of the Elastic-Plastic Contact Problem. To solve the set of Eq. 1.19–1.26, displacements in equation 1.21 should be related to the initial state and to the contact pressure increment. Equations 1.22 and 1.23 show that the first two terms can be expressed with p, δp, and ε^p. The third term, δu_3^r, is expressed as a function of the plastic strain increment $\delta\varepsilon^p$.

Plastic Strain Increment. Equations 1.18, 1.24, and 1.25 can be put together, leading to Eq. 1.27, showing that plastic strain increment depends upon p, ε^p, δp, hardening parameters and $\delta\varepsilon^p$ itself.

$$\delta\varepsilon^p = f(p, \varepsilon^p, \delta p, \delta\varepsilon^p, \text{ hardening parameters}) \tag{1.27}$$

An iterative procedure (Gauss-Seidel iterative method) must be used to obtain plastic strain increment, solution of Eq. 1.27, and depending of p, ε^p, δp, fulfilling the conditions described above.

The algorithm described in Fig. 4 is used to evaluate the plastic strain increment. Contact pressure p, contact pressure increment δp, plastic strain ε^p and hardening parameters are all known. The pressure stress σ^{pr}, pressure stress increment $\delta\sigma^{pr}$ and residual stress σ^r can be calculated, and the residual stress increment is initialized to zero.

An initial plastic strain increment $\delta\varepsilon^{pi}$ is calculated, using the chosen plasticity model. The residual stress increment is evaluated and used to compute a new plastic strain increment $\delta\varepsilon^{pf}$, that is compared with $\delta\varepsilon^{pi}$. The convergence is obtained when $|\delta\varepsilon^{pf} - \delta\varepsilon^{pi}|/\max|\delta\varepsilon^{pi}| < \text{eps}$ and checked by calculating the final Von Mises stress which should be equal to the final micro-yield stress at every point of the plastic zone (also called the consistency condition). If the convergence is not obtained, a new initial plastic strain increment is calculated from $\delta\varepsilon^{pi}$ and $\delta\varepsilon^{pf}$. This process is repeated until convergence is reached. Once convergence is obtained, the plastic strain increment is accurately estimated and takes into account the evolution of stress with plastic flow.

Elastic-Plastic Contact Resolution Algorithm. To solve the incremental elastic-plastic contact problem, the algorithm presented Fig. 5 will be used.

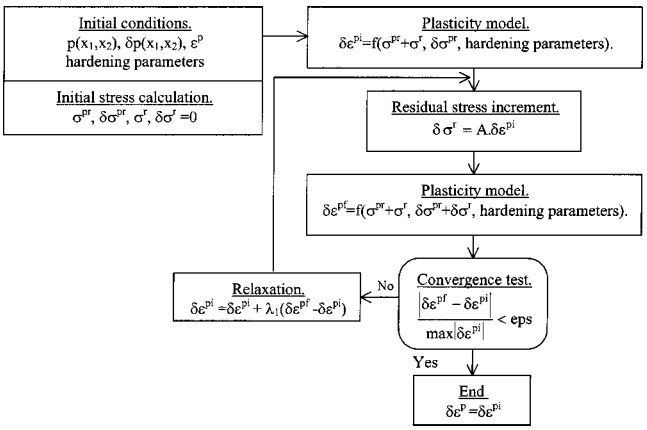

Fig. 4 Plastic strain increment algorithm

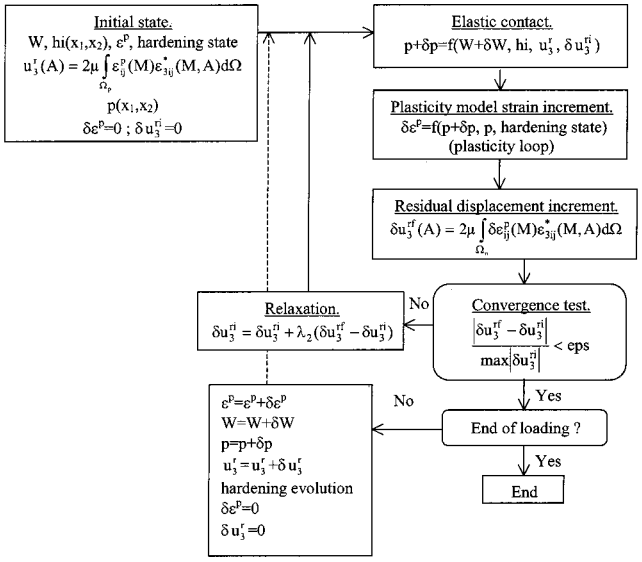

Fig. 5 Elastic-plastic contact problem resolution algorithm

Starting from the initial conditions defined by the load W, the initial geometry $hi(x_1,x_2)$, the existing plastic deformation and the associated residual displacement u_3^r, the contact pressure and by the hardening state of the bodies in contact, the elastic contact problem is solved, taking into account the load increment. From this load increment, the plastic strain increment is obtained (Fig. 4), enabling the calculation of the residual displacement increment, which is then compared with the one that has been used for the contact pressure calculation. The convergence is reached when $|\delta u_3^{rf}-\delta u_3^{ri}|/\max|\delta u_3^{ri}|<$eps and the validity of the solution is evaluated by observing the pressure distribution, the residual displacement of the surface points and the residual stress and strain state below the surface. If the convergence is not obtained, it is re-entered into the elastic contact resolution. This process is repeated until the residual displacement increment converges. Plastic strains, load, contact pressure, residual displacement and hardening parameters are then increased by their increment to define a new initial condition for the next loading step.

The elastic-plastic contact formulation has been established, as well as the algorithm to solve the problem. It is now necessary to present the methods established to perform the different calculations.

2 Development of Calculation Tools

It can be seen in the algorithms presented in Figs. 4 and 5 that four calculations need to be performed. First, it is necessary to solve the elastic contact problem with any initial geometry. Second, residual displacements must be evaluated from the plastic strains. Third, residual stress and finally the pressure stress must be obtained.

2.1 Elastic Contact Problem Resolution. The determination of the contact pressure will be done using a normal dry elastic point contact code written by Coulon [21] using multigrid techniques as proposed by Lubrecht and Ioannides [14]. This contact code solves the set of equations composed of the load balance Eq. (1.1), the contact conditions (1.3) and the elastic surface separation equation, with any initial geometry:

$$h(x_1,x_2)=himod(x_1,x_2)+\delta+u_3^{pr(B1+B2)}(x_1,x_2)\,. \quad (2.1)$$

2.2 Residual Displacements. The residual displacements due to plastic strains are given by Eq. 1.23 and 1.24. To allow a numerical resolution of the problem, the volume where plastic strains have non zero value (Ω_p) is divided into N_v elementary cuboids Ω_{cn}. The displacements generated by those N elementary cuboids can be written:

$$u_3^r(A)=2\mu\sum_{n=1}^{N_v}\int_{\Omega_{cn}}\varepsilon_{ij}^p(M).\varepsilon_{3ij}^*(M,A)d\Omega\,. \quad (2.2)$$

In each cuboid, plastic strains are considered constant. Expression 2.2 then becomes:

$$u_3^r(A)=2\mu\sum_{n=1}^{N_v}\varepsilon_{ij}^p(n)\int_{\Omega_{cn}}\varepsilon_{3ij}^*d\Omega=\sum_{n=1}^{N}\varepsilon_{ij}^p(n)D_{3ij}(n) \quad (2.3)$$

$$\text{with}\quad D_{3ij}=\mu\int\int\int_{\Omega_{cn}}(u_{3i,j}^*+u_{3j,i}^*)dx_1dx_2dx_3\,. \quad (2.4)$$

To calculate residual displacements of the surface, expressions given in Eq. 2.3 and 2.4 must be integrated. Consider a point A (Fig. 6) on the surface with a force of magnitude unity acting normally to the half-space surface and a cuboid of plastic strain $2\Delta x_1.2\Delta x_2.2\Delta x_3$ large. The cuboid of plastic strain has center $C(c_1,c_2,c_3)$ in a mark attached to point A. The displacements generated by this force are given for every point $M(x_1,x_2,x_3)$ of the half-space by (Love, [22]):

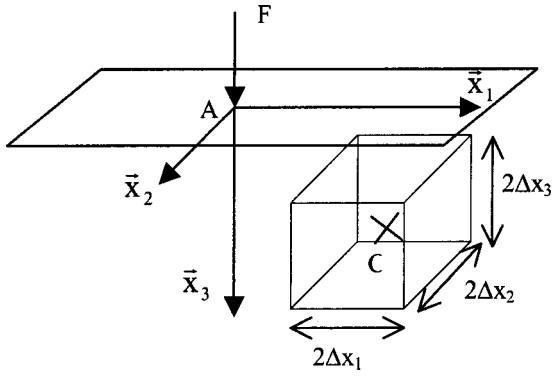

Fig. 6 Cuboid of constant plastic strain

$$4\pi\mu\begin{pmatrix} u^*_{31} \\ u^*_{32} \\ u^*_{33} \end{pmatrix} = \frac{1-2\nu}{r}\begin{bmatrix} \frac{x_1.x_3}{r^3} - \frac{(1-2\nu).x_1}{r(x_3+r)} \\ \frac{x_2.x_3}{r^3} - \frac{(1-2\nu).x_2}{r(x_3+r)} \\ \frac{x_3^2}{r^3} + \frac{2(1-\nu)}{r} \end{bmatrix} \quad \text{with}$$

$$r = \sqrt{x_1^2+x_2^2+x_3^2}. \tag{2.5}$$

If functions F_{ij} are defined so that $\partial F_{ij}(x_1,x_2,x_3)/\partial x_1\partial x_2\partial x_3 = \mu(u^*_{3i,j}+u^*_{3j,i})$, then functions D_{3ij} are expressed by:

$$\begin{aligned} D_{3ij} = {} & F_{ij}(c_1+\Delta x_1,c_2+\Delta x_2,c_3+\Delta x_3) - F_{ij}(c_1+\Delta x_1,c_2 \\ & +\Delta x_2,c_3-\Delta x_3) - F_{ij}(c_1+\Delta x_1,c_2-\Delta x_2,c_3+\Delta x_3) \\ & + F_{ij}(c_1+\Delta x_1,c_2-\Delta x_2,c_3-\Delta x_3) - F_{ij}(c_1-\Delta x_1,c_2 \\ & +\Delta x_2,c_3+\Delta x_3) + F_{ij}(c_1-\Delta x_1,c_2+\Delta x_2,c_3-\Delta x_3) \\ & + F_{ij}(c_1-\Delta x_1,c_2-\Delta x_2,c_3+\Delta x_3) - F_{ij}(c_1-\Delta x_1,c_2 \\ & -\Delta x_2,c_3-\Delta x_3). \end{aligned} \tag{2.6}$$

Functions F can be integrated and expressed by:

$$F_{11}(x,y,z) = \frac{1}{\pi}\left[-\nu x\ln(y+R) - (1-2\nu)z\tan^{-1}\left(\frac{y+z+R}{x}\right)\right]$$

$$F_{22}(x,y,z) = \frac{1}{\pi}\left[-\nu y\ln(x+R) - (1-2\nu)z\tan^{-1}\left(\frac{x+z+R}{y}\right)\right]$$

$$F_{12}(x,y,z) = \frac{1}{\pi}[-2\nu R - (1-2\nu)z\ln(z+R)]$$

$$F_{13}(x,y,z) = \frac{1}{\pi}\left[2x\tan^{-1}\left(\frac{y+z+R}{x}\right) + y\ln(z+R)\right] \tag{2.7}$$

$$F_{23}(x,y,z) = \frac{1}{\pi}\left[2y\tan^{-1}\left(\frac{x+z+R}{y}\right) + x\ln(z+R)\right]$$

$$F_{33}(x,y,z) = \frac{1}{2\pi}\left[2(1-\nu)\left(2z\tan^{-1}\left(\frac{x+y+R}{z}\right) + x\ln(y+R) + y\ln(x+R)\right) - \frac{z}{2}\theta\right]$$

$$\text{with} \quad \theta = -2.\tan^{-1}\left(\frac{xy}{zR}\right) \quad \text{and} \quad R = \sqrt{x^2+y^2+z^2}.$$

Residual displacements of the surface due to plastic strains existing in the half-space can now be computed, using the relations described above.

2.3 Residual Stresses. Residual stresses are the stresses generated by plastic strains in a half-space where the surface is free of any load ($p_i(M)=0$ in Eq. 1.17). The volume where plastic strains are not nil (Ω_p) is divided as in section 2.2 in N_v elementary cuboids of constant plastic strain. The residual stress at a point is the sum of the contribution of all elementary cuboids.

The calculation of residual stresses is based on the work of Chiu [23,24]. Residual stresses at a point $M(x_1,x_2,x_3)$ in a half-space due to a cuboid of constant plastic strain, whose center C has coordinates $(0,0,h)$ are obtained by the relation:

$$\sigma^r_{ij}(M) = A_{ijkl}(M,C)\varepsilon^p_{kl}(C). \tag{2.8}$$

The tensor A includes 36 different terms, expressed in Appendix 1. This tensor depends on x_1,x_2,x_3, but also on the depth h of the cuboid of constant plastic strain.

2.4 Pressure Stresses. To calculate pressure stresses, the surface is discretized in a rectangular mesh. On each element, the pressure has a constant value. Influence coefficients taken from Vergne [25] and given in Appendix 2 give the stresses induced by a rectangular cell on a half-space submitted to an uniform pressure. If the contact zone Γ_c is divided in N cells, the stress at a point $M(x1,x2,x3)$ is obtained by

$$\sigma^{pr}(M) = \sum_{n=1}^{N} p(A_n).G(\overrightarrow{A_nM}), \tag{2.9}$$

where A_n is the control point of cell n.

Every calculation needed to solve the elastic-plastic contact problem, following the algorithm described in Figs. 4 and 5 have been described. The SAC must now be evaluated and compared with other numerical tools.

2.5 Calculation Speed. The direct calculation of contact pressure, residual displacements, residual stresses and pressure stresses requires numerous operations to be performed, as can be seen in Table 1, where N_{vz} is the number of points of the plastic volume in depth, and N_{vs} is the number of points in the plastic volume per depth. The use of accelerating techniques, such as multigrid and FFT strongly reduced the computational cost of those calculations [26]. The benefit of the limitation of the discretized volume to the plastic region is also very important, since the number of operations required to calculate residual stresses increases with N^2_{vz}.

To give an idea of the computational cost, for one load step, about 10 contact loops (see Fig. 5) are required with each time between 80 (first contact loops) down to 5 (last contact loops) plasticity loops (see Fig. 4), giving a total of about 300 plasticity loops. Thus, a typical problem of a moving load rolling on a smooth surface with 24×24 points along the x and y directions, respectively, and with about $140\times20\times11$ points in the plastic zone, with a rolling movement divided in 170 time step, can be solved in approximately 4600 seconds on a 1 GHz Personal Computer.

For partial comparison, using the FE method with the commercial code ABAQUS, one load step for an axisymmetric configuration (to simulate only vertical loading) with 2600 elements requires 300 seconds on a 552 MHz powerstation. Extension to large strains and rotations, or to three-dimensional contact problems is also possible. However the rolling over a surface defect seems difficult to obtain with the current version of the software (but should be possible using another commercial software package).

3 Validation of the SAC

A computer program has been written, following the methodology proposed above. First, a plasticity model has been chosen. This choice, as described in paragraph 3.1 has been made according the material the authors want to work on. Second, the nano indentation test with a spherical punch has been studied. This test, which can be simulated by FE, is used to validate the SAC. Last the SAC is applied to three problems, showing the capability of the SAC to answer the problem of the dented rolling contact.

Table 1 Optimization of the calculation time

	Direct method	Accelerated method (technique)	
Contact pressure	N_s^2	$N_s \ln N_s$	(multigrid)
Residual displacement	$N_{vz}N_{vs}N_s$	$N_{vz}(N_s+N_{vs})\ln(N_s+N_{vs})$	(FFT)
Residual stress	$N_{vz}{}^2N_{vs}{}^2$	$N_{vz}{}^2N_{vs}\ln N_{vs}$	(FFT)
Pressure stress	$N_sN_{vz}N_{vs}$	$N_{vz}(N_s+N_{vs})\ln(N_s+N_{vs})$	(FFT)

3.1 Plasticity Model. There are numerous models of plasticity available, each having different capabilities to describe various experimental phenomena. To choose among those various models, the following considerations are made.

The SAC is mainly dedicated to simulate contact between bodies made of bearing steel. One of the characteristic of those steels is that the slope of the hardening curve is high at the beginning of the curve, and then continuously decreases. Therefore, the linear kinematic hardening model that can not represent this phenomena is eliminated.

The kinematic hardening of steels is important when the stress is reversed during cyclic loading. The SAC is devoted to contact calculation, where it is not the case. Furthermore, this code must simulate contact with bodies made of surface hardened steel, and it is difficult to identify hardening parameters. So, a simple model of isotropic hardening has been chosen. Tresca and Von Mises criteria are very close to each other and both give a correct representation of the yield surface. For numerical reasons, Von Mises criterion is used, and the model chosen is that of Prandtl-Reuss.

The hardening law is described by the Swift's law

$$\sigma_{VM} = B.(C+\varepsilon^p)^n. \tag{3.1}$$

The plastic flow law can then be formulated according to Lamaître and Chaboche [27] as follows:

$$\delta\varepsilon = \delta\varepsilon^e + \delta\varepsilon^p$$

$$\delta\varepsilon^e = \frac{1+\nu}{E}\,\delta\sigma - \frac{\nu}{E}(\mathrm{Tr}(\delta\sigma))I$$

$$\text{if} \quad \begin{matrix} f=0 \quad \text{and} \quad \delta f=0 \\ (f=\sigma_{VM}-\sigma_Y) \end{matrix} \left| \begin{matrix} \delta\varepsilon^p = \dfrac{3}{2}g'(\sigma_{VM})\dfrac{\delta\sigma_{VM}}{\sigma_{VM}}\sigma' \quad \text{with} \quad g'(\sigma_{VM}) = [k'(k^{-1}(\sigma_{VM}))]^{-1} \\ \delta\varepsilon^p = 0 \quad \text{otherwise} \qquad\qquad \sigma = k(\varepsilon^p) \ \text{ is the hardening law} \end{matrix} \right.$$

$$\text{with the Swift's law:} \quad g'(\sigma_{VM}) = \frac{1}{n.B}\left(\frac{B}{\sigma_{VM}}\right)^{1-1/n}. \tag{3.2}$$

σ' is the deviatoric stress tensor; σ_{VM} is the von Mises stress. The symbol $'$ stands for derivative with respect to the argument.

The choice of this model is relevant to the materials the authors want to work on. However, it is important to note that another choice of modeling is always possible and that only the module that calculates plastic strains has to be changed, the other steps being identical.

3.2 Validation of the SAC. Nano Indentation Test. To confirm the results supplied by the SAC, a comparison with the commercial finite element code ABAQUS is made. First, it is necessary to solve properly the same problem by both methods. Since the SAC simulates the contact between two half-spaces, at first the FE results are compared with the Hertz theory (assuming an elastic behavior of the bodies). Next, the elastic-plastic FE analysis is compared with the results supplied by the SAC. To fully validate the SAC, the nano-indentation test will be studied. In this test, surface geometry changes have a non-negligible effect on the pressure field, plastic flow has an important influence on the stress field and small strain theory can be used. Furthermore, experimental data are available, enabling an experimental validation of the results supplied by the SAC.

Problem Definition. The test problem will be the nano-indentation of a steel whose elastic characteristics are $E=210$ GPa and $\nu=0.3$ for Young modulus and Poisson coefficient. Its plastic behavior is described by the Swift's law whose parameter are $B=1240$ MPa, $C=30$, and $n=0.085$. The plastic strain is expressed in 10^{-6} deformation. These values are taken according to El Ghazal [19] and they correspond to the experimental data presented later in this paragraph. The body made of steel is smooth and flat.

The punch is a sphere of 105 μm radius made of diamond. In the simulations, the punch can be assumed rigid or having an elastic behavior, with $E=1140$ GPa and $\nu=0.07$.

Resolution of an Identical Problem by FE. The code developed here is in the framework of Hertz's hypotheses; so it is necessary to simulate with ABAQUS, the contact between two half-spaces. For this, three simulations have been conducted. In this section, only the elastic behavior of the bodies in contact is considered.

First, a Hertzian pressure is applied on a half-space. The mesh is refined in the contact zone (90 nodes in contact), and limit conditions are zero displacement at infinity, by the use of infinite elements. The problem is axisymetric. The displacement of the surface is then compared with results supplied by Hertz theory (Fig. 7). Both solutions seems almost identical. It validates the choice of the boundary conditions imposed on the mesh.

In a second step, a rigid punch is in contact with the half-space. The variation of the load with the rigid body displacement is

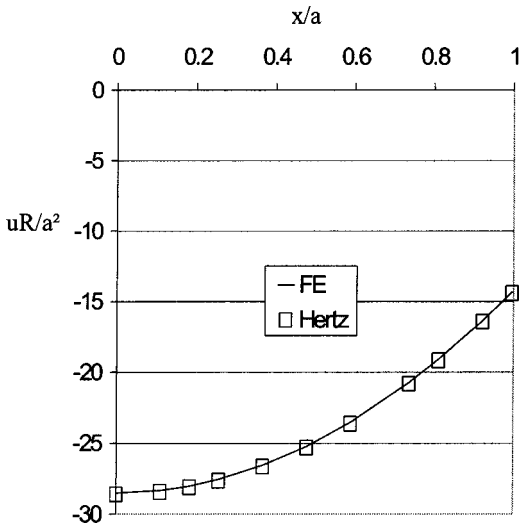

Fig. 7 Dimensionless normal surface displacement under load for a Hertzian pressure versus dimensionless distance from center of symmetry

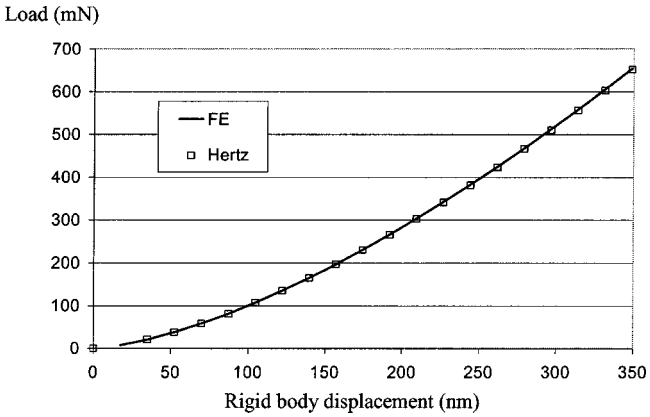

Fig. 8 Load versus rigid body displacement. Rigid punch.

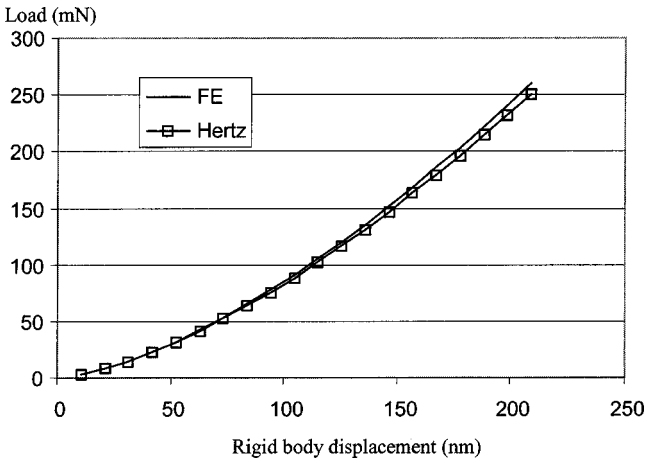

Fig. 9 Load versus rigid body displacement. Deformable punch.

plotted in Fig. 8. The Hertz solution is identical to the results given by the FE simulation, and therefore, the contact is correctly solved by the FE code.

Finally, the contact between an half-space and a deformable punch made of diamond is studied. The results, plotted in Fig. 9, show a difference between the FE analysis and the analytical solution. This difference has essentially two origins: As the punch is truncated (Fig. 10), the half-space hypotheses are not respected. Furthermore, the load is imposed by moving vertically the nodes at the top of the mesh, which disables the warping of this plane. So the contact between a rigid punch and a half-space will be used to validate the SAC.

Validation of the SAC. In order to validate the results supplied by the SAC, simulations have been carried out with an elastic-plastic body in contact with a rigid punch and the solution is observed in several ways.

First, the evolution of the load with the rigid body displacement is plotted in Fig. 11. The results supplied by the FE code and by the SAC are identical. The formed indent has a depth of about 80 nm. Because the hardening model that has been chosen, no plasticity occurs during unloading. Therefore, the comparison of the unloading of the elastic indentation and the unloading of the elastic-plastic indentation shows the influence of the geometry change. If the geometry would not change, the pressure would be the same in both cases, and the two unloading curves should be only shifted. This can also be seen in Fig. 12, where the elastic Hertzian pressure for a load of 650 mN is compared with that

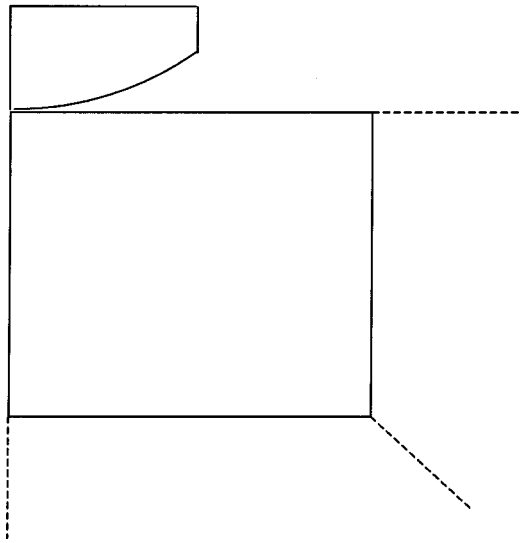

Fig. 10 Meshing of the elastic punch

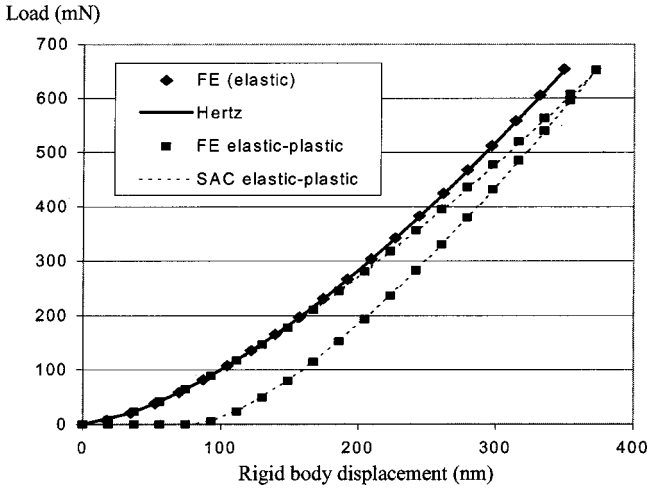

Fig. 11 Load versus rigid body displacement. Rigid punch and elastic-plastic half-space.

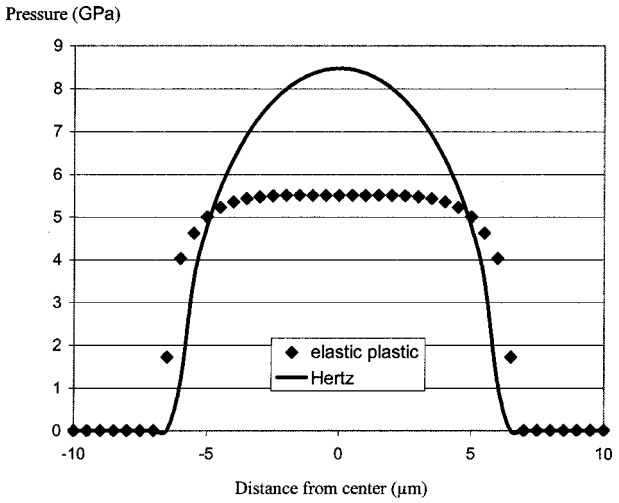

Fig. 12 Influence of plasticity on pressure distribution. Load of 650 mN.

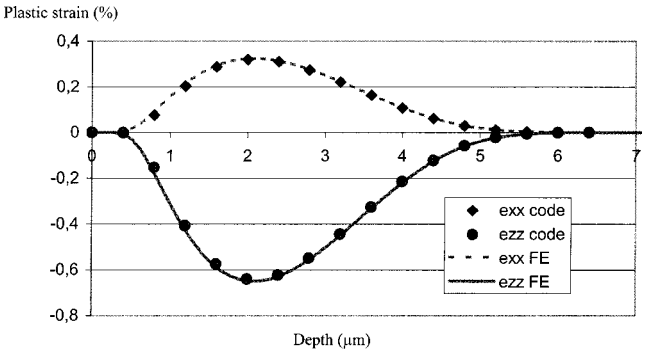

Fig. 13 Plastic strain versus depth along the contact axis

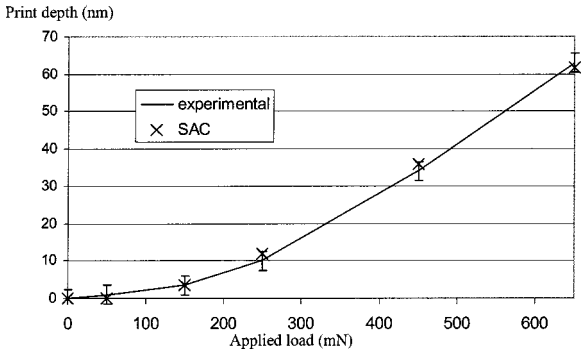

Fig. 17 Residual print depth versus applied load [28]

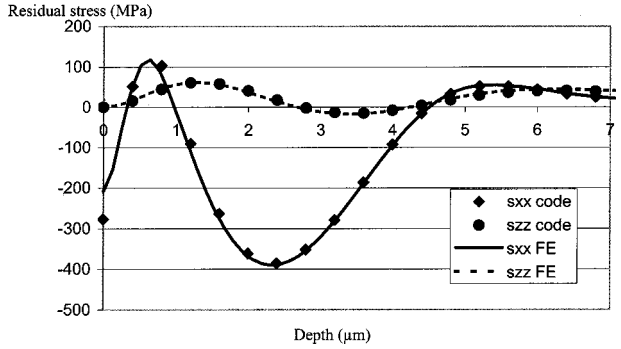

Fig. 14 Residual stress versus depth along the contact axis

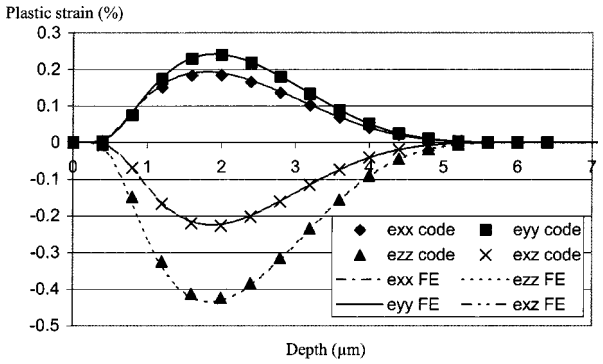

Fig. 15 Plastic strain profile at 2 microns far from the contact axis

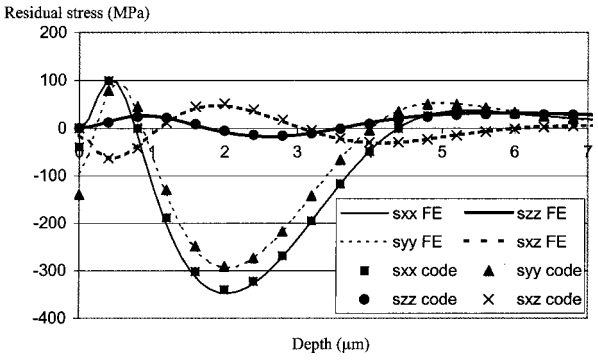

Fig. 16 Residual stress profile at 2 microns far from the contact axis

obtained in the elastic-plastic case, and illustrates why it is necessary to take into account the surface modification during the resolution of the elastic-plastic contact problem.

Plastic strains and residual stresses along the contact axis are plotted respectively in Figs. 13 and 14 for SAC and FE code. The applied load is 190 mN. First, good agreement between the results supplied by both tools for plastic strains as well as for residual stresses is noticed. The maximum plastic strain for this case is about 0.6 percent, and can reach 1.5 percent under a load of 650 mN. The small strain theory is still valid, but for higher loads, this hypothesis might not hold. Figure 14 shows that the σ_{xx} stress is much more important than the σ_{zz} stress (influence of the surface) and that the value obtained for residual stresses are not negligible. If this contact was purely elastic, the Hertz's pressure would be of 4.9 GPa, leading to a maximum shear stress of 1470 MPa.

Finally, Figs. 15 and 16, which represent respectively plastic strains and residual stresses along a profile two microns far from the contact axis (which correspond approximately to $0.25\times a$, a being the contact radius), show also a good agreement between the different results.

A comparison was also made with experimental data, obtained from a nano-indentation test carried by El Ghazal [19], where the measurement process has been numerically reproduced. Experimental data and numeric simulations agree very well, as shown in Fig. 17. For this simulation, the punch was elastic, with elastic properties of diamond ($E=1140$ GPa and $\nu=0.07$).

3.3 Application of the SAC. To illustrate the capabilities of the SAC, three applications are presented. First, the rolling on a smooth surface is presented. Second, the case of the vertical loading of a dented surface and last the rolling on a dented surface have been studied.

Rolling on a Smooth Surface. To illustrate the capabilities of the SAC, a smooth rolling contact between an elastic sphere and an elastic-plastic half-space is presented. The elastic sphere is made of steel ($E=210$ GPa and $\nu=0.3$) and the elastic-plastic half-space properties are the same as in the previous part. The sphere has a radius of 20 mm, and the applied load is 4200 N, that leads to a Hertz pressure of 3 GPa and a contact radius of 820 μm. The surface displacement at the center of the rolling track after unloading is shown in Fig. 18. The contact is first loaded to 5000 N, then the load is maintained constant and the sphere is rolled on the elastic-plastic half-space on the distance of 4200 μm, and the contact is finally unloaded (position 0 is the center of the contact at this moment). It can be seen that the sphere must be rolled over about two times the contact radius to be in steady state. The results are intentionally presented in a dimensional form, since the behavior depends not only of the elastic limit, but also on the hardening law parameters.

Vertical Loading of a Dented Surface. The case of the vertical loading of the dented contact is considered. The dent (Fig. 19) is

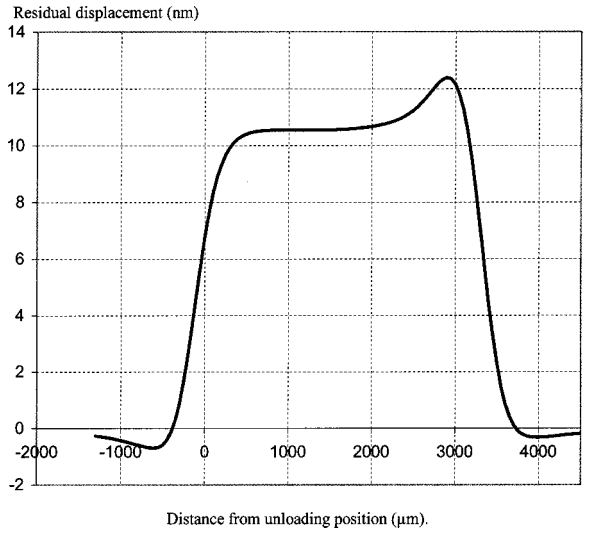

Fig. 18 Surface displacement at the center of the rolling track after unloading

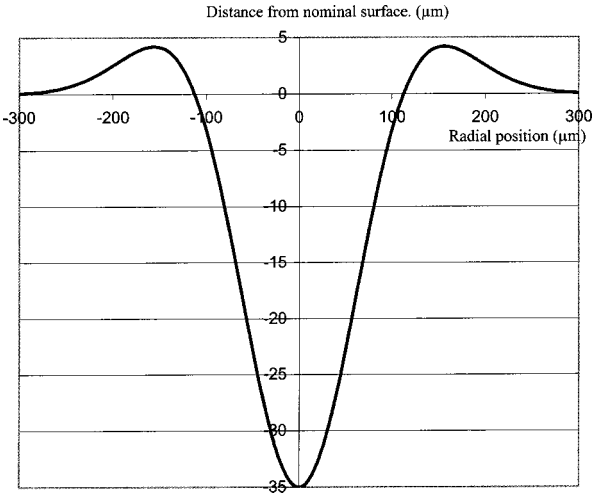

Fig. 19 Dent geometry

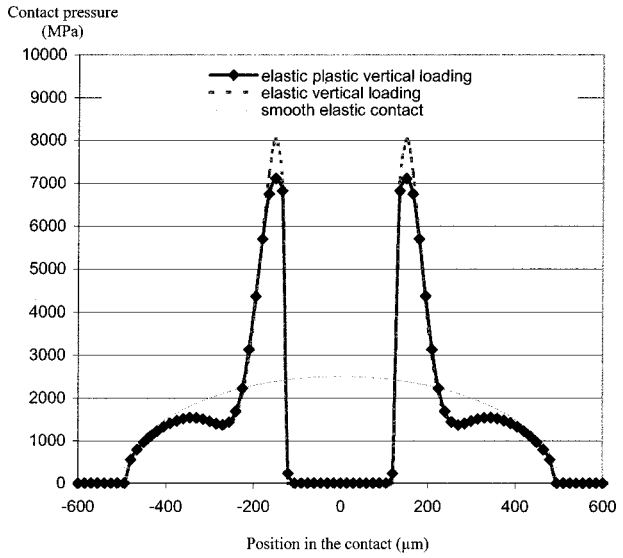

Fig. 20 Elastic and elastic-plastic dented contact. Contact pressure.

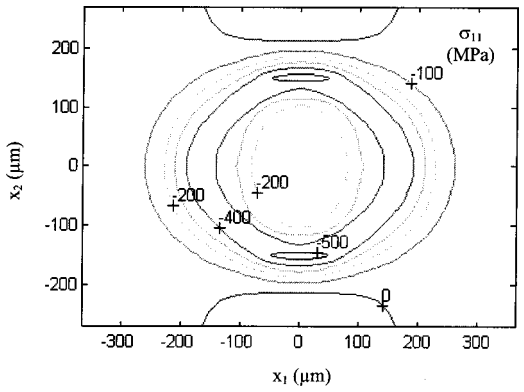

Fig. 21 Residual stress σ_{11} in MPa in the plane $x_3=65\ \mu$m

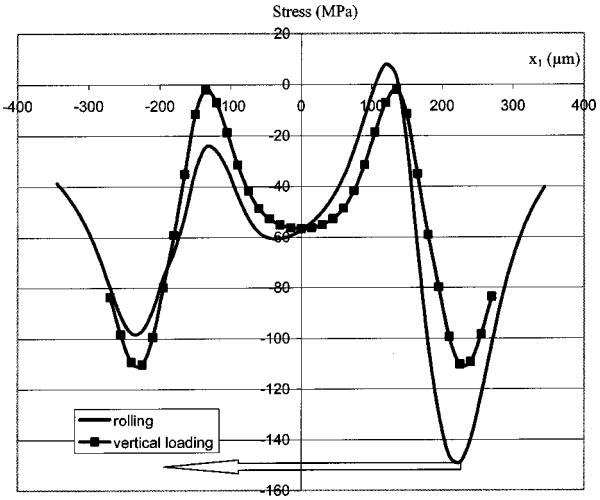

Fig. 22 Residual stress σ_{11} in MPa. Profile at $x_2=0$; $x_3=75\ \mu$m. Comparison between vertical loading and rolling.

described by a damped cosinus, that described a dent of 35 μm depth and of 115 μm radius, with shoulders 4 μm height.

$$hi(x,y)=hi(x,y)+35\cos\left[2\pi\frac{450}{r}\right]\exp\left[-13\frac{r^2}{450^2}\right]. \quad (3.3)$$

The dented body is made of steel, whose characteristics are $E=219$ GPa, $\nu=0.3$, $B=1280$ MPa, $C=4$, and $n=0.095$. It is a sphere of 24 mm radius. The smooth body is elastic, with a Young modulus, $E=210$ GPa, and a Poisson coefficient, $\nu=0.3$, and is a sphere of 40 mm radius. The load applied to the bodies in contact is $W=1318$ N, leading to a Hertz pressure of 2.5 GPa, and to a contact area radius of $a=500\ \mu$m for a smooth elastic contact.

The pressure field obtained with an elastic analysis and with an elastic-plastic analysis are both plotted in Fig. 20. It can be seen that the presence of the dent at the center of the contact strongly modified the pressure repartition from the smooth case. The plastic effect is visible on the pressure peaks, that are about 10 percent more important when predicted by the elastic analysis than when they are estimated with the elastic-plastic analysis.

The residual stress field can also be obtained as shown in Fig. 21 where σ_{11}^r is plotted in the plane x_3 (i.e., depth)$=50\ \mu$m. It can be seen to be important (down to -500 MPa), and consequently can strongly modify the stress field associated with contact pressure.

Rolling on a Dented Surface. In this part, the loading history is modified. The load is applied when the dent is not in the contact area. The initial geometry is smooth, and the contact is elastic

under a load of 2.5 GPa. The bodies in contact are then rolled. The dent enters the contact, and plastic strains appear. The bodies are rolled until the dent leaves the contact area.

After the rolling on a dented surface, contact pressure and surface geometry are close to that obtained after the vertical loading. However, the distribution of plastic strains and residual stresses can be different. The difference between the two cases can be seen in Fig. 22. The residual stress σ_{11} is plotted along the rolling direction and is perfectly symmetric in the vertical loading case. The stress becomes disymmetric in the rolling case, and the minimum σ_{11} residual stress is increased by nearly 30 percent. That result can explain why spalling occurs usually ahead of the dent (along the direction of the load movement) considering the beneficial effect of the compressive residual stress on the fatigue life.

4 Conclusion

A three-dimensional semi-analytical elastic-plastic contact code has been developed. Hertz and small strain hypotheses have been used, and further simplifications have not been made. This tool has been validated by comparison with numerical results supplied by a FE commercial code. A special care has been brought to the contact resolution by FE. A comparison has also been carried out with experimental data from a nano-indentation test, and the agreement in both cases is very good. The main advantage of this code over classical FE codes is the reduction of the calculation time, making transient analysis of three dimensional contact problems affordable, including when a fine mesh is required.

Opportunities given by this SAC are very wide. First, initial residual stresses can be introduced. The analysis enables the influence of asymmetric residual stress on microyield stress measurement by nano-indentation (vertical loading) to be studied, following the method developed by El Ghazal [28]. In a second step, since initial hardening and hardening parameters changing with depth can be introduced, this SAC is a convenient tool to analyze the dented contact between two rolling bodies. The capability to treat the dented contact under vertical loading as well as under rolling conditions has been developed. These two applications are of primarily interest for the study of the rolling contact fatigue of steel with a dented surface. Eventually, this tool should also be useful to better understand the influence of the indentation process on RCF mechanisms.

Appendix 1

Residual Stress Calculation. In this appendix, the expressions allowing to calculate residual stresses from plastic strains in a half-space are given. More details are given by Chiu [15,16]. The tensor A includes 36 different terms:

$$\begin{bmatrix} \sigma^r_{11} \\ \sigma^r_{22} \\ \sigma^r_{33} \\ \sigma^r_{12} \\ \sigma^r_{13} \\ \sigma^r_{23} \end{bmatrix} = \begin{bmatrix} A_{111} & A_{1122} & A_{1133} & A_{1112} & A_{1113} & A_{1123} \\ A_{2211} & A_{2222} & A_{2233} & A_{2212} & A_{2213} & A_{2223} \\ A_{3311} & A_{3322} & A_{3333} & A_{3312} & A_{3313} & A_{3323} \\ A_{1211} & A_{1222} & A_{1233} & A_{1212} & A_{1213} & A_{1223} \\ A_{1311} & A_{1322} & A_{1333} & A_{1312} & A_{1313} & A_{1323} \\ A_{2311} & A_{2322} & A_{2333} & A_{2312} & A_{2313} & A_{2323} \end{bmatrix} \begin{bmatrix} \varepsilon^p_{11} \\ \varepsilon^p_{22} \\ \varepsilon^p_{33} \\ \varepsilon^p_{12} \\ \varepsilon^p_{13} \\ \varepsilon^p_{23} \end{bmatrix}$$

The solution is calculated as the superposition of three solutions (Fig. 23).

Solution 1 corresponds to the solution in an infinite space in presence of a cuboid of constant plastic strain.

Solution 2 corresponds to the solution in an infinite space in the presence of a mirror cuboid of constant plastic strain, such as plastic deformations ε^p_{13} and ε^p_{23} are set opposites from those of the main element. The superposition of the two solutions leaves the median plane free of tangential stresses.

Finally, Solution 3 corresponds to a half-space on which is applied the field of normal stress obtained on the median plane from Solutions 1 and 2 which is the double of each solution taken separately. At the end, the desired solution of a half-space in the presence of a cuboid of constant plastic strains with a free surface is obtained.

Solutions 1 and 2 are expressed in a mark bound to the center of the cuboid of plastic strain by $\sigma_{ij}=B_{ijkl}\varepsilon^p_{kl}$. Solution 3 is expressed in a mark whose origin is placed on the surface by $\sigma_{ij}=P_{ijkl}\varepsilon^p_{kl}$.
The final solution is expressed by:

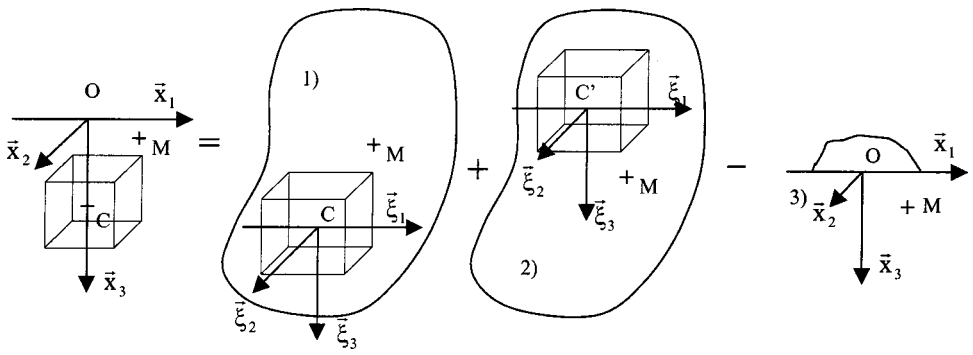

Fig. 23 Superposition of solutions

$$\begin{bmatrix}\sigma_{11}^r\\ \sigma_{22}^r\\ \sigma_{33}^r\\ \sigma_{12}^r\\ \sigma_{13}^r\\ \sigma_{23}^r\end{bmatrix}=A(x_1,x_2,x_3,h)\begin{bmatrix}\varepsilon_{11}^p\\ \varepsilon_{22}^p\\ \varepsilon_{33}^p\\ \varepsilon_{12}^p\\ \varepsilon_{13}^p\\ \varepsilon_{23}^p\end{bmatrix}$$

$$=B(x_1,x_2,x_3-h)\begin{bmatrix}\varepsilon_{11}^p\\ \varepsilon_{22}^p\\ \varepsilon_{33}^p\\ \varepsilon_{12}^p\\ \varepsilon_{13}^p\\ \varepsilon_{23}^p\end{bmatrix}$$

$$+B(x_1,x_2,x_3+h)\begin{bmatrix}\varepsilon_{11}^p\\ \varepsilon_{22}^p\\ \varepsilon_{33}^p\\ \varepsilon_{12}^p\\ -\varepsilon_{13}^p\\ -\varepsilon_{23}^p\end{bmatrix}$$

$$-P(x_1,x_2,x_3,h)\begin{bmatrix}\varepsilon_{11}^p\\ \varepsilon_{22}^p\\ \varepsilon_{33}^p\\ \varepsilon_{12}^p\\ -\varepsilon_{13}^p\\ -\varepsilon_{23}^p\end{bmatrix}.$$

Stress Calculation in an Infinite Space. An infinite space is considered (Figs. 16-1, 16-2). Consider the mark $(C,\vec{\xi}_1,\vec{\xi}_2,\vec{\xi}_3)$, bound to the center of the cuboid of size $2\Delta x_1.2\Delta x_2.2\Delta x_3$. Consider a point $M(\xi_1,\xi_2,\xi_3)$. The coordinates of the vectors linking the corners of the element to this point are noted

$$\vec{C_m}=(\gamma_1^m,\gamma_2^m,\gamma_3^m)$$

$$\vec{C_1}=(\xi_1-\Delta x_1,\xi_2-\Delta x_2,\xi_3-\Delta x_3)$$

$$\vec{C_2}=(\xi_1+\Delta x_1,\xi_2-\Delta x_2,\xi_3-\Delta x_3)$$

$$\vec{C_3}=(\xi_1+\Delta x_1,\xi_2+\Delta x_2,\xi_3-\Delta x_3)$$

$$\vec{C_4}=(\xi_1-\Delta x_1,\xi_2+\Delta x_2,\xi_3-\Delta x_3)$$

$$\vec{C_5}=(\xi_1-\Delta x_1,\gamma_2+\Delta x_2,\xi_3+\Delta x_3)$$

$$\vec{C_6}=(\xi_1-\Delta x_1,\xi_2-\Delta x_2,\xi_3+\Delta x_3)$$

$$\vec{C_7}=(\xi_1+\Delta x_1,\xi_2-\Delta x_2,\xi_3+\Delta x_3)$$

$$\vec{C_8}=(\xi_1+\Delta x_1,\xi_2+\Delta x_2,\xi_3+\Delta x_3).$$

Elastic strains at point M generated by a cuboid of constant and unity plastic strain ε_{11}^p are given by:

$$\varepsilon_{1111}=\frac{1}{8\pi^3}\sum_{m=1}^{8}\left[D_{,1111}^m+\frac{2-\nu}{1-\nu}(D_{,1122}^m+D_{,1133}^m)\right]-H(M)$$

$$\varepsilon_{2211}=-\frac{1}{8\pi^3}\sum_{m=1}^{8}-D_{,1122}^m+\frac{\nu}{1-\nu}(D_{,2222}^m+D_{,2233}^m)$$

$$\varepsilon_{3311}=-\frac{1}{8\pi^3}\sum_{m=1}^{8}-D_{,1133}^m+\frac{\nu}{1-\nu}(D_{,2233}^m+D_{,3333}^m)$$

$$\varepsilon_{1211}=\frac{1}{8\pi^2}\sum_{m=1}^{8}\frac{\nu}{1-\nu}D_{,1112}^m+\frac{1+\nu}{1-\nu}(D_{,2221}^m+D_{,3312}^m)$$

$$\varepsilon_{1311}=\frac{1}{8\pi^3}\sum_{m=1}^{8}\frac{\nu}{1-\nu}D_{,1113}^m+\frac{1+gn}{1-\nu}(D_{,3331}^m+D_{,2213}^m)$$

$$\varepsilon_{2311}=\frac{1}{8\pi^3}\sum_{m=1}^{8}\frac{\nu}{1-\nu}(D_{,2223}^m+D_{,3332}^m).$$

In the presence of unity shear strain $(\varepsilon_{12}^p+\varepsilon_{21}^p)=2$, elastic deformations at point M are given by:

$$\varepsilon_{1112}=\frac{1}{8\pi^3}\sum_{m=1}^{8}\frac{-2\nu}{1-\nu}D_{,1112}^m+2(D_{,2221}^m+D_{,3312}^m)$$

$$\varepsilon_{2212}=\frac{1}{8\pi^3}\sum_{m=1}^{8}\frac{-2\nu}{1-\nu}D_{,1222}^m+2(D_{,1112}^m+D_{,3312}^m)$$

$$\varepsilon_{3312}=\frac{1}{8\pi^3}\sum_{m=1}^{8}\frac{-2\nu}{1-\nu}D_{,3312}^m$$

$$\varepsilon_{1212}=\frac{1}{8\pi^3}\sum_{m=1}^{8}\left[\frac{-2\nu}{1-\nu}D_{,1122}^m+D_{,1111}^m+D_{,2222}^m+D_{,1133}^m+D_{,2233}^m\right]-H(M)$$

$$\varepsilon_{1312}=\frac{1}{8\pi^3}\sum_{m=1}^{8}-\frac{1+\nu}{1-\nu}D_{,1123}^m+D_{,2223}^m+D_{,3332}^m$$

$$\varepsilon_{2312}=\frac{1}{8\pi^3}\sum_{m=1}^{8}-\frac{1+\nu}{1-\nu}D_{,2213}^m+D_{,1113}^m+D_{,3331}^m.$$

With $H(M)=1$ if M is inside the cuboid and $H(M)=0$ otherwise.

The functions D are defined by:

$$D_{,1111}^m=2\pi^2\left[\tan^{-1}\left[\frac{\gamma_2^m\gamma_3^m}{\gamma_1^m R}\right]-\frac{\gamma_1^m\gamma_2^m\gamma_3^m}{2R}\left(\frac{1}{\gamma_1^{m^2}+\gamma_2^{m^2}}+\frac{1}{\gamma_1^{m^2}+\gamma_3^{m^2}}\right)\right]$$

$$D_{,1112}^m=-\pi^2\left[(\gamma_3^m).\ln\left(\frac{R+|\gamma_3^m|}{(\gamma_1^{m^2}+\gamma_2^{m^2})^{1/2}}\right)-\frac{\gamma_1^{m^2}\gamma_3^m}{(\gamma_1^{m^2}+\gamma_2^{m^2})R}\right]$$

$$D_{,1122}^m=\frac{\pi^2\gamma_1^m\gamma_2^m\gamma_3^m}{(\gamma_1^{m^2}+\gamma_2^{m^2})R}\quad\text{with}\quad R=\sqrt{\gamma_1^{m^2}+\gamma_2^{m^2}+\gamma_3^{m^2}}$$

$$D_{,1123}^m=-\frac{\pi^2\gamma_1^m}{R}.$$

The rest of derivatives are obtained by circular permutation of the subscripts.

From Hooke's law, it is then possible to find out stresses and so to determine the components of the tensor B for every point M.

Expression of the Solution (3). The cuboid of constant strains has a size of $2\Delta x_1.2\Delta x_2.2\Delta x_3$. The coordinates of the vector linking the corners of the mirror element to the projection of M on the plane $(O,\vec{x}_1,\vec{x}_2)$ are noted $\vec{C_m}=(c_{mx},c_{my},c_{mz})$

$$\vec{C_1}=(x_1-\Delta x_1,x_2-\Delta x_2,h-\Delta x_3)$$

$$\vec{C_2}=(x_1+\Delta x_1,x_2-\Delta x_2,h-\Delta x_3)$$

$$\vec{C_3}=(x_1+\Delta x_1,x_2+\Delta x_2,h-\Delta x_3)$$

$$\vec{C_4}=(x_1-\Delta x_1,x_2+\Delta x_2,h-\Delta x_3)$$

$$\vec{C_5}=(x_1-\Delta x_1,x_2+\Delta x_2,h+\Delta x_3)$$

$$\vec{C_6}=(x_1-\Delta x_1,x_2-\Delta x_2,h+\Delta x_3)$$

$$\vec{C_7}=(x_1+\Delta x_1,x_2-\Delta x_2,h+\Delta x_3)$$

$$\vec{C_8}=(x_1+\Delta x_1,x_2+\Delta x_2,h+\Delta x_3)$$

The terms of the tensor P can be expressed with:

$$\begin{bmatrix} P_{xxkl} \\ P_{yykl} \\ P_{zzkl} \\ P_{xykl} \\ P_{xzkl} \\ P_{yzkl} \end{bmatrix} = 2. \begin{bmatrix} -z.f_{kl}(0,2,1)+f_{kl}(0,2,2)+2\nu f_{kl}(2,0,2) \\ -z.f_{kl}(2,0,1)+f_{kl}(2,0,2)+2\nu f_{kl}(0,2,2) \\ f_{kl}(0,0,0)+z.f_{kl}(0,0,-1) \\ (1-2\nu).f_{kl}(1,1,2)-z.f_{kl}(1,1,1) \\ -i.z.f_{kl}(0,1,0) \\ -i.z.f_{kl}(1,0,0) \end{bmatrix}$$

with

$$f_{kl}(r,s,q)=\sum_{m=1}^{8}(-1)^m\int\int_{-\infty}^{+\infty}\frac{\overline{\sigma}_{kl}(x,y,c_{mz})\exp[-\chi z+i(\xi_2 c_{mx}+\xi_3 c_{my})\xi_2^r\xi_3^s d\xi_2 d\xi_3}{\chi^q}.$$

$$\text{and}\quad \chi=\sqrt{\xi_2^2+\xi_3^2}.$$

These functions f_{kl} can be expressed as the sum of functions $V_{u,n,k}$

$$\begin{aligned} f_{xx}(0,0,0)=\frac{\lambda}{8\pi^2}\sum_{m=}^{8}\Bigg\{ & -V_{-1,-1,0}(z+c_{mz})+V_{3,-1,4}(z+c_{mz})-V_{3,-1,4}(z)+\frac{c_{mz}}{2}(V_{-1,-1,-1}(z+c_{mz}) \\ & +V_{3,-1,3}(z+c_{mz}))-\frac{V_{-1,1,1}(z+c_{mz})}{1-\nu}-\frac{4\nu-1-2\nu^2}{2\nu(1-\nu)}\frac{c_{mz}}{2}V_{1,-1,1}(z+c_{mz}) \\ & +\frac{\nu}{1-\nu}.\left(V_{-1,3,4}(z+c_{mz})-V_{-1,3,4}(z)+\frac{C_{mz}}{2}V_{-1,3,3}(z+c_{mz})\right) \\ & +\frac{1}{-\nu}\left(V_{1,1,4}(z+c_{mz})-V_{1,1,4}(z)+\frac{c_{mz}}{2}V_{1,1,3}(z+c_{mz})\right)\Bigg\}. \end{aligned}$$

f_{yy} (0, 0, 0) deducts by permuting the subscripts u and n of functions $V_{u,n,k}$

$$\begin{aligned} f_{zz}(0,0,0)=\frac{\lambda}{8\pi^2}\sum_{m=1}^{8}\Bigg\{ & -\frac{1-\nu}{\nu}\left[V_{-1,-1,0}(z+c_{mz})+\frac{c_{mz}}{2}V_{-1,-1,-1}(z+c_{mz})\right] \\ & +\frac{\nu}{1-\nu}\left[\begin{array}{c} 2V_{1,1,4}(z+c_{mz})+C_{mz}V_{1,1,3}(z+c_{mz})+V_{3,-1,4}(z+c_{mz})+V_{-1,3,4}(z+c_{mz}) \\ +\frac{c_{mz}}{2}(V_{3,-1,3}(z+c_{mz})+V_{-1,3,3}(z+c_{mz}))-2V_{1,1,4}(z)-V_{3,-1,4}(z)-V_{-1,3,4}(z) \end{array}\right]\Bigg\} \end{aligned}$$

$$f_{xy}(0,0,0)=\frac{\lambda}{8\pi^2}\sum_{m=1}^{8}(1-2\nu).\left(\frac{V_{0,0,1}(z+c_{mz})}{\nu}+\frac{C_{ml}V_{0,0,1}(z+c_{mz})+2.(V_{0,0,2}(z+c_{mz})-V_{0,0,2}(z))}{1-\nu}\right)$$

$$f_{xz}(0,0,0)=\frac{\lambda}{8\pi^2}\sum_{m=1}^{8}\frac{1-2\nu}{\nu(1-\nu)}(V_{0,-1,1}(z+c_{mz})+C_{ml}V_{0,-1,0}(z+c_{mz})).$$

f_{yz} (0, 0, 0) deducts by permuting the subscripts u and n of functions $V_{u,n,k}$. f_{xy}, f_{xz}, and f_{yz} take into account the symmetry of the plastic deformations tensor. Functions f_{kl} (r,s,q) deduct from f_{kl} (0, 0, 0) by adding r, s, and q on the corresponding subscripts of function $V_{u,n,k}$.

The functions $V_{u,n,k}$ are given by:

$$V_{u,n,k}=\int\int_{-\infty}^{+\infty}\frac{\exp[-\chi z+i(\xi_2 c_{mx}+\xi_3 c_{my})\xi_2^u\xi_3^n d\xi_2 d\xi_3}{\chi^k}$$

$$V_{0,0,k}=2\pi J_{1-k,0}$$

$$V_{0,1,k}=2\pi i\sin\Phi.J_{2-k,1}$$

$$V_{1,1,k}=-2\pi\sin\Phi.\cos\Phi.J_{3-k,2}\quad \rho=\sqrt{x^2+y^2};\quad \Phi=\tan^{-1}(y/x)$$

$$V_{0,2,k}=\pi[J_{3-k,0}+\cos(2\Phi).J_{3-k,2}]$$

$$V_{2,2,k}=\pi/4[J_{5-k,0}-\cos(4\Phi).J_{5-k,4}]$$

$$V_{0,3,k}=(\pi/2)i\sin\Phi[3J_{4-k,1}-(4\sin^2\Phi-3).J_{4-k,3}]$$

$$V_{1,3,k}=\pi\sin 2\Phi[\sin^2\Phi J_{5-k,0}+(3-8\sin^2\Phi)\rho^{-1}.J_{4-k,1}-12\cos(2\Phi)\rho^{-2}J_{3-k,2}].$$

$J_{n,m}=\int_0^\infty r^n e^{-rz}J_m(\rho r)dr=\Gamma(n+m+1)/(\rho^2+z^2)^{(n+1)/2}P_n^{-m}(z/\sqrt{\rho^2+z^2})$, where P_n^{-m} is the associated Legendre polynomial and J is the Bessel function of the first kind.

When $(n+m+1)=0$, this function is not defined. The function $J_{-m-1,m}=\int_0^\infty (e^{-rz}-1)J_m(\rho r)/r^{m+1}dr=\int_0^z\int_0^\infty -e^{-rz}J_m(\rho r)/r^m dr$ will be used instead

$$V_{-1,0,1}=2\pi i H_{1,0}$$

$$V_{-1,0,0}=2\pi i z H_{3,0}$$

$$V_{-1,0,-1}=2\pi i(3z^2H_{5,0}-H_{3,0})$$

$$V_{-1,1,1}=-2\pi H_{3,0}$$

$$V_{-1,1,0}=-6\pi yzH_{5,0}$$

$$V_{-1,1,2}=-2\pi y(H_{0,2}-zH_{1,2})$$

and functions H are:

$$H_{0,2}=\frac{\tan^{-1}(x/y)}{y}$$

$$H_{1,2}=\frac{\tan^{-1}(xz/y\sqrt{z^2+\rho^2})}{zy}$$

$$H_{3,0}=\frac{x}{(y^2+z^2)\sqrt{z^2+\rho^2}}$$

$$H_{1,0}=\ln\frac{x+\sqrt{z^2+\rho^2}}{(y^2+z^2)^{1/2}}$$

$$H_{5,0}=\frac{y^2+z^2}{3}\left[2H_{3,0}+\frac{x}{(z^2+\rho^2)^{3/2}}\right].$$

Finally, functions V follow the recursive relation:

$$V_{u+2,n,k}+V_{u,n+2,k}=V_{u,n,k-2}$$

The different components of tensor P can then be computed.

Appendix 2

Stress Calculation in a Half-Space Loaded on Surface. For an element of uniform normal pressure P of size $2a.2b$ centered on the origin O, stresses at a point $M(x_1,x_2,x_3)$ are given by (Vergne [17]):

$$\sigma_{ij}^{pr}=\frac{P}{2\pi}G_{ij}(\overrightarrow{OM})$$

$$\sigma_{ij}^{pr}=\frac{P}{2\pi}[g_{ij}(x_1+a,x_2+b,x_3)-g_{ij}(x_1+a,x_2-b,x_3)+g_{ij}(x_1-a,x_2-b,x_3)-g_{ij}(x_1-a,x_2+b,x_3)].$$

The functions g are defined by:

$$g_{11}(x,y,z)=2\nu\tan^{-1}\left(\frac{z^2+y^2-\rho y}{zx}\right)+2(1-\nu)\tan^{-1}\left(\frac{\rho-y+z}{x}\right)+\frac{xyz}{\rho(x^2+z^2)}$$

$$g_{22}(x,y,z)=2\nu\tan^{-1}\left(\frac{z^2+y^2-\rho y}{zx}\right)+2(1-\nu)\tan^{-1}\left(\frac{\rho-x+z}{y}\right)+\frac{x_1yz}{\rho(y^2+z^2)}$$

$$g_{33}(x,y,z)=\tan^{-1}\left(\frac{z^2+y^2-\rho y}{zx}\right)-\frac{x_1yz}{\rho}\left(\frac{1}{x^2+z^2}+\frac{1}{y^2+z^2}\right)$$

$$g_{12}(x,y,z)=-\frac{z}{\rho}-(1-2\nu)\ln(\rho+z)$$

$$g_{13}(x,y,z)=\frac{z^2y}{\rho(x^2+z^2)}$$

$$g_{23}(x,y,z)=\frac{z^2x}{\rho(y^2+z^2)}$$

with $\rho=\sqrt{x^2+y^2+z^2}$.

References

[1] Lamagnère, P., Fougères, R., Lormand, G., Vincent, A., Girodin, D., Dudragne, G., and Vergne, F., 1998, "A Physically Based Model for Endurance Limit of Bearing Steels," ASME J. Tribol., **120**, pp. 421–426.

[2] Barber, J. R., and Ciavarella, M., 2000, "Contact Mechanics," Int. J. Solids Struct., **37**, pp. 29–43.

[3] Tichy, J. A., and Meyer, D. M., 2000, "Review of Solid Mechanics in Tribology," Int. J. Solids Struct., **37**, pp. 391–400.

[4] Archard, J. F., Hunt, R. T., and Onions, R. A., 1975, "Stylus Profilometry and the Analysis of the Contact of Rough Surfaces," *The Mechanics of the Contact Between Deformable Bodies*, Delft University Press, pp. 282–303.

[5] Greenwood, J. A., and Williamson, J. B. P., 1966, "Contact of Nominally Flat Surfaces," Proc. R. Soc. London, Ser. A, **295**, pp. 300–319.

[6] Zhao, Y. W., Maietta, D. M., and Chang, L., 2000, "An Asperity Microcontact Model Incorporating the Transition from Elastic Deformation to Fully Plastic Flow," ASME J. Tribol., **122**, pp. 86–93.

[7] Hahn, G. T., Bhargava, V., Rubin, C. A., Chan, Q., and Kim, K., 1987, "Analysis of the Rolling Contact Residual Stresses and Cyclic Plastic Deformation of SAE 52100 Steel Ball Bearings," ASME J. Tribol., **109**, pp. 618–626.

[8] Gupta, V., Hahn, G. T., Bastias, P. C., and Rubin, C. A., 1995, "Contribution of Surface Irregularities to Rolling Contact Plasticity in Bearing Steels," ASME J. Tribol., **117**, pp. 660–666.

[9] Dang Van, K., and Maitournam, M. H., 1993, "Steady-State Flow in Classical Elastoplasticity: Applications to Repeated Rolling and Sliding Contact," J. Mech. Phys. Solids, **41**(11), pp. 1691–1710.

[10] Hearle, A. D., and Johnson, K. L., 1987, "Cumulative Plastic Flow in Rolling and Sliding Line Contact," ASME J. Appl. Mech., **54**, pp. 1–7.

[11] Virmoux, P., Inglebert, G., and Gras, R., 1994, "Characterisation of Elastic-Plastic Behaviour for Contact Purposes on Surface Hardened Materials," *Proc., 20th Leeds-Lyon Symposium on Tribology*, Lyon, France, 7–10 September 1993, Tribology series, Elsevier, **27**, pp. 287–301.

[12] Mayeur, C., Sainsot, P., and Flamand, L., 1995, "A Numerical Elastoplastic Model for Rough Contact," ASME J. Tribol., **117**, pp. 422–429.

[13] Polonsky, I. A., and Keer, L. M., 2000, "A Fast and Accurate Method for Numerical Analysis of Elastic Layered Contacts," ASME J. Tribol., **122**, pp. 30–35.

[14] Lubrecht, A. A., and Ioannides, E., 1991, "A Fast Solution for the Dry Contact Problem and the Associated Subsurface Stress Field, Using Multilevel Techniques," ASME J. Tribol., **113**, pp. 128–133.

[15] Xu, G., Sadeghi, F., and Hoeprich, M., 1997, "Residual Stresses Due to Debris Effects in EHL Contacts," Tribol. Trans., **40**, pp. 613–621.

[16] Liu, G., Wang, Q., and Liu, S., 2001, "A Three-Dimensional Thermal-Mechanical Asperity Contact Model for Two Nominally Flat Surfaces in Contact," ASME J. Tribol., **123**, pp. 595–602.

[17] Jacq, C., Lormand, G., Vincent, A., Nélias, D., and Dudragne, G., "On the Influence of Residual Stresses on the Determination of the Microplasticity Properties of a Nitrided Steel by Nano-Indentation," to appear in Materials Science and Engineering.

[18] Brebbia, L. C., 1980, *The Boundary Element Method for Engineers*, Pentech Press, London.

[19] Mayeur, C., 1995, "Modélisation du contact rugueux élastoplastique," Ph.D. Thesis, INSA Lyon, France.

[20] Blomerus, P. M., Hills, D. A., and Kelly, P. A., 1999, "The Distributed Dislocation Method Applied to the Analysis of Elastoplastic Strain Concentrations," J. Mech. Phys. Solids, **47**, pp. 1007–1026.

[21] Coulon, S., Ville, F., and Nélias, D., 2001, "Numerical and Experimental Investigations on Rolling Contact Fatigue for Dented Surfaces," *Proc., 27th Leeds-Lyon Symposium on Tribology*, Lyon, France, 5–8 September 2000, Tribology series, Elsevier, **39**, pp. 459–467.

[22] Love, A. E. H., 1952, *A Treatise on the Mathematical Theory of Elasticity*, 4th Ed. Cambridge University Press, Cambridge.

[23] Chiu, Y. P., 1978, "On the Stress Field and Surface Deformation in a Half-Space With a Cuboidal Zone in which Initial Strains Are Uniform," ASME J. Appl. Mech., **45**, pp. 302–306.

[24] Chiu, Y. P., 1977, ''On the Stress Field due to Initial Strains in a Cuboid Surrounded by an Infinite Elastic Space,'' ASME J. Appl. Mech., **44**, pp. 587–590.
[25] Vergne, F., 1985, ''Calcul des déplacements et des contraintes dans un demi-espace élastique chargé en surface par des actions distribuées normales et tangentielles quelconques,'' M.Sc. Thesis, INSA Lyon, France.
[26] Sainsot, P., Jacq, C., and Nélias, D., ''A Numerical Model for Elastoplastic Rough Contact,'' to appear in Computer Modeling in Engineering & Sciences.
[27] Lemaître, L., Chaboche, J. L., 1988, *Mécanique des matériaux solides*, Dunod, Paris.
[28] El Ghazal, H., 1999, ''Etude des propriétés microstructurales et mécaniques des aciers 16NiCrMo13 cémenté et 32CrMoV13 nitruré-Application à la prévision de leur limite d'endurance en fatigue de roulement,'' Ph.D. Thesis, INSA Lyon, France.